Journal of Zhejiang University-SCIENCE C (Computers & Electronics)
ISSN 1869-1951 (Print); ISSN 1869-196X (Online)
www.zju.edu.cn/jzus; www.springerlink.com
E-mail: jzus@zju.edu.cn

Design and derivation of the dual transponder carrier ranging system

Ming-chen ZHAO[†], Chun-hui WANG[†‡], Zhong-he JIN

(*Department of Information Science and Electronic Engineering, Zhejiang University, Hangzhou 310027, China*)

[†]E-mail: {doublefish, hytgwch}@zju.edu.cn

Received Sept. 17, 2012; Revision accepted Feb. 27, 2013; Crosschecked Apr. 17, 2013

Abstract: The accuracy of microwave ranging is mainly limited by the frequency instability of the oscillator that generates the carrier phase signal. A dual transponder carrier ranging method is used to minimize the oscillator noise by combining the reference and the to-and-fro measurements. This ranging approach together with pseudo-noise ranging or other means can be used to measure the inter-satellite distance with a high precision. The pseudo-noise ranging system or other ranging systems help to solve the integer circles while the dual transponder ranging system guarantees the accurate fractional circle. The two satellites work in the master-slave mode. The range measurements are derived on the master satellite while the slave satellite just coherently transfers the received signal, so that the dual transponder ranging system does not need to rely on the time tagging system to synchronize the two satellites. This study first describes the dual transponder carrier ranging system and shows how the system removes most of the oscillator noise components effectively. Then, a detailed design scheme on the frequency planning of the ranging system is presented and the supporting analysis illustrates the feasibility of this system. Based on the design innovation, a laboratory demonstration system is assembled to verify the realizability of the dual transponder ranging system. The experimental results demonstrate that a high level of accuracy (about 30 μm under laboratory circumstance) can be achieved by the use of the proposed dual transponder carrier ranging system.

Key words: Inter-satellite, Carrier ranging, Oscillator noise, High precision, Ranging accuracy
doi:10.1631/jzus.C1200266 **Document code:** A **CLC number:** TN927

1 Introduction

High accuracy measurement of the inter-satellite distance has become increasingly important in satellite formation flying. One traditional way of measuring the distance between satellites is to use a microwave ranging system to count the number of carrier phase cycles in the one-way flight time. However, the ranging accuracy of such a system is mainly limited by the instability of the oscillator that drives the carrier-phase signals (Kim, 2007). To improve the ranging accuracy, a dual one-way ranging (DOWR) system has been explored. This ranging system could minimize the oscillator noise effect by combining the one-way range measurements from two microwave ranging systems. The frequency fluctuations caused by oscillator instability have nearly equal and opposite effects on each satellite's phase measurement, and most of the oscillator noise would be canceled when summing these two phases simultaneously (Kim, 2000; Kim and Tapley, 2003).

The gravity recovery and climate experiment (GRACE) adopted this DOWR system to measure the inter-satellite distance changes with μm-level accuracy (Bertiger *et al*., 2002). The GRACE mission, consisting of two co-orbiting satellites separated by about 220 km, was successfully launched in March 2002. It was designed to map the Earth's gravity field with a high precision (Thomas, 1999; Kim and Tapley, 2002). Each satellite was equipped with the following instruments (Bertiger *et al*., 2003): a K-band ranging

‡ Corresponding author

(KBR) system, a global positioning system (GPS) receiver, an ultra-stable oscillator (USO), an accelerometer, and two star trackers; among all these instruments, the KBR system was the most important one. One should note that the KBR system is another name of the GRACE DOWR system since it uses K (24-GHz) and Ka (32-GHz) band frequencies (Kim and Tapley, 2005).

Although the DOWR system can achieve a high level of accuracy, it has a disadvantage that the DOWR must rely on a time tagging system to synchronize the twin satellites. Time mismatching of the twin satellites will degrade the noise cancellation performance and decrease the ranging accuracy accordingly. Take the GRACE mission for example. The time-tag synchronization requirement was less than 150 ps, and the GRACE onboard GPS receiver was used to provide the required time-tag information (Kim, 2000). In practice, the synchronization requirement limits the DOWR system applications to post-processing missions, and a time-consuming algorithm is needed to perform the interpolation of the time-tag correction process. Therefore, the two measurement phases of the twin satellites as well as the time-tag information need to be recorded and transmitted to a control segment, such as the ground station. On the whole, the processing procedure of the DOWR system is complicated and it is not suitable for real-time use. Afterwards, to mitigate the time-synchronization requirement, an optimal frequency configuration had been proposed by Kim and Tapley (2005). Unfortunately, implementation of the optimal frequency configuration was at the expense of increasing the hardware cost.

Based on the principle of minimizing the oscillator noise by the DOWR system, the dual transponder carrier ranging system was proposed (Zhao *et al*., 2009). This ranging system can also achieve a high level of accuracy by minimizing the oscillator noise. Moreover, it does not need to rely on the time tagging system. However, previous study has mainly focused on the fundamental model of the ranging system, while theory analysis is still scarce when considering the implementation of the dual transponder ranging system. Consequently, it is necessary to provide more studies to verify the feasibility of the dual transponder ranging system.

With respect to several sources of noises in carrier ranging, such as oscillator noise, system noise, and multipath noise, Zhao *et al*. (2009) carried out a comprehensive simulation test and the results indicated that the main error source for microwave ranging systems was the oscillator noise. Furthermore, according to DOWR, the carrier ranging accuracy was mainly limited by the instability of the oscillator that drove the phase signals (Macarthur and Posner, 1985; Kim, 2000). Therefore, it seems reasonable that the oscillator noise is the main error source in carrier ranging systems. In our study, we primarily focus on the oscillator instability since it is the dominant factor. Further studies will be concerned with other error sources (such as system noise, multipath noise, ionosphere phase shift, and phase distortion), the operating distance, and the dynamic limitation.

The aim of this paper is to provide a novel design scheme of the dual transponder ranging system so as to minimize the oscillator noise.

2 Measurement model

This section overviews the dual transponder ranging system. Fig. 1 illustrates the derivation of the phase measurements from the dual transponder carrier ranging system. According to the principle of dual transponder ranging, the two satellites work in the master-slave mode. In Fig. 1, the 1st satellite represents the master satellite and the 2nd satellite represents the slave satellite. The range measurements are derived on the master satellite while the slave satellite just coherently transfers the received signal. For this reason, the dual transponder ranging system presents a major advantage that it does not need to rely on the time tagging system to synchronize the two satellites.

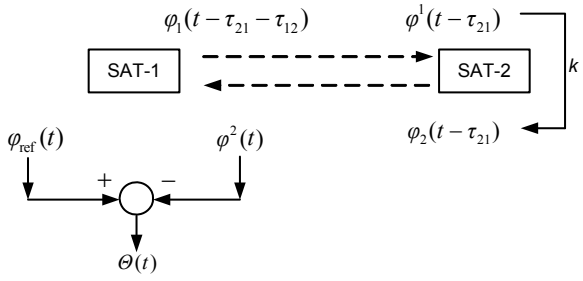

Fig. 1 Phase measurements of the dual transponder ranging system

Theoretically, the master satellite generates a measurement phase from a USO, which travels to the slave satellite. The measurement phase is then coherently transferred by the slave satellite and comes back to the master, where it is subtracted from the reference phase. Since the two phases are fundamentally generated from the same USO, combining these two phases tends to cancel most of the oscillator noise.

The following deduction shows how the biased range is obtained and how the oscillator noise is canceled out through the use of the dual transponder carrier ranging system.

The frequency carrier phase measurement received at a nominal time t can be modeled as

$$\Theta(t)=\varphi_{\mathrm{ref}}(t)-\varphi^{2}(t)+E, \tag{1}$$

which is the difference between the reference phase of the 1st satellite $\varphi_{\mathrm{ref}}(t)$ and the received phase from the 2nd satellite $\varphi^{2}(t)$. The remaining term E is the combination of the integer ambiguity, ionosphere phase shift, phase shift caused by other effects, and measurement noise (Kim, 2007).

The received phase can be replaced with the transmitted phase, offset in time by the one-way propagation delay between the two satellites:

$$\begin{cases}\varphi^{2}(t)=\varphi_{2}(t-\tau_{21}),\\ \varphi^{1}(t-\tau_{21})=\varphi_{1}(t-\tau_{12}-\tau_{21}),\end{cases} \tag{2}$$

where τ_{12} is the flight time from the 1st satellite to the 2nd satellite, and τ_{21} is the flight time from the 2nd satellite to the 1st satellite.

The 2nd satellite receives the phase from the 1st satellite, completes the scaling transformation, and transmits the processed phase. Conventionally, the coherent transfer maintains synchronization. The proportionality constant from the output phase to the input phase is assumed to be k. Note that k is a preliminarily defined constant. At the same time, the reference phase of the 1st satellite synchronizes with the transmitted phase of the 1st satellite, and the scale factor is also k (Zhao *et al*., 2009):

$$\begin{cases}\varphi_{2}(t-\tau_{21})=k\varphi^{1}(t-\tau_{21}),\\ \varphi_{\mathrm{ref}}(t)=k\varphi_{1}(t).\end{cases} \tag{3}$$

Substituting Eqs. (2) and (3) into Eq. (1), the phase measurement can be presented by

$$\Theta(t)=k\varphi_{1}(t)-k\varphi_{1}(t-\tau_{12}-\tau_{21})+E, \tag{4}$$

which can be expanded after appropriate substitutions and approximations are made. Each phase $\varphi(t)$ can be decomposed into the reference phase $\bar{\varphi}$ and the phase error $\delta\varphi$ caused by the oscillator instability (Kim and Tapley, 2003). The phase at the transmitted time $t-\tau_{12}-\tau_{21}$ can be linearized around the phase at the nominal time t as (Zhao *et al*., 2009)

$$\begin{cases}\bar{\varphi}_{1}(t-\tau_{12}-\tau_{21})\approx\bar{\varphi}_{1}(t)-\dot{\bar{\varphi}}_{1}(t)(\tau_{12}+\tau_{21}),\\ \delta\varphi_{1}(t-\tau_{12}-\tau_{21})\approx\delta\varphi_{1}(t)-\delta\dot{\bar{\varphi}}_{1}(t)(\tau_{12}+\tau_{21}).\end{cases} \tag{5}$$

The rate of phase change $\dot{\bar{\varphi}}_{1}(t)$ can be replaced by the nominal frequency of the transmitted signal of the 1st satellite f_1, and the rate of phase error change $\delta\varphi_1(t)$ is equivalent to the frequency error $\delta f_1(t)$ (Kim and Tapley, 2003). After these substitutions, Eq. (4) can be approximated by

$$\Theta(t)=kf_{1}(\tau_{12}+\tau_{21})+k\delta f_{1}(\tau_{12}+\tau_{21})+E, \tag{6}$$

where the first term represents the true phase measurement, and the second term represents the phase error caused by the oscillator errors.

The two times of flight, τ_{12} and τ_{21}, are slightly different. The first term in Eq. (6) can be converted into a single time-of-flight (TOF) corresponding to the instantaneous range $\rho(t)$ by the use of

$$\begin{aligned}f_{1}(\tau_{12}+\tau_{21})&\approx 2f_{1}\tau+\Delta\Theta_{\mathrm{TOF}},\\ \tau&=\rho(t)/c,\end{aligned} \tag{7}$$

where $\Delta\Theta_{\mathrm{TOF}}$ is called a light-time range correction. An algorithm has been developed to solve this light-time range correction (Kim, 2000).

The phase measurement is converted to a dual transponder range by multiplication with an effective wavelength λ:

$$\begin{aligned}R(t)&\equiv\lambda\Theta(t),\\ \lambda&=c/(2kf_{1}).\end{aligned} \tag{8}$$

The instantaneous range $\rho(t)$ can be related to the dual transponder range measurement $R(t)$ when substituting Eqs. (7) and (8) into Eq. (6):

$$R(t)=\rho(t)+\rho_{\mathrm{TOF}}(t)+\rho_{\mathrm{err}}(t)+\rho_E(t), \tag{9}$$

where ρ_{TOF} is the light-time range correction, ρ_{err} is the range error caused by the oscillator, and ρ_E is obtained by scaling the remaining term E with λ.

In summary, the biased range can be derived from the phase measurement of the dual transponder ranging system. From the second term of Eq. (6), we can conclude that the frequency instability in the dual transponder carrier ranging system contains only the drift in TOF. This implies that the long and medium period oscillator errors which have a period longer than the TOF can be removed effectively.

Although the model seems possible, the immediate question is how to construct this ranging system. According to the principle of dual transponder carrier ranging, a reference phase is needed in the derivation of the combined phase measurement. In other words, the reference signal needs to be produced at the same time of the transmitted signal. However, the frequency of the reference signal is just the same as the received signal transferred by the other satellite, and thus the reference signal can leak into the receiver input. Obviously, in this case, severe interference will occur between the two signals and the results will not be acceptable. Besides, how to complete the scaling transformation on the slave satellite is another challenge that needs to be conquered. With regard to these issues, a feasible design scheme is presented in the next section.

3 System design

In this section, we first briefly introduce the characteristic of phase-locked loops (PLLs), which is essential for our design analysis. Then, details on the design scheme are discussed, which mainly focus on the frequency planning of the two satellites on the premise of the relative motionless condition. Thereafter, the dynamics are taken into consideration.

3.1 Phase-locked loops

3.1.1 Frequency synthesizer

PLL is usually served as a frequency multiplier for its superiority in noise suppression. The basic PLL structure is shown in Fig. 2.

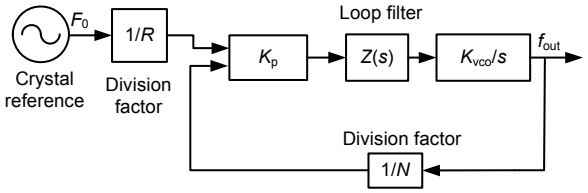

Fig. 2 Basic phase-locked loop (PLL) structure

Based on the property of PLL, the output frequency f_{out} satisfies the relationship $f_{\mathrm{out}}/F_0=N/R$. In other words, the PLL can be served as a frequency synthesizer to generate the required frequency from the reference signal.

Introduce the open loop transfer function:

$$G(s)=\frac{K_{\mathrm{p}}\cdot K_{\mathrm{vco}}\cdot Z(s)}{s}, \tag{10}$$

where K_{p} is the gain of the phase discriminator, K_{vco} is the gain of VCO, and $Z(s)$ is the passive loop filter (Dean, 2003). To simplify calculation, assume H=1/N. Using the standard control theory, the transfer function which relates the VCO output to the output of the crystal reference is derived as

$$\frac{1}{R}\frac{G(s)}{1+G(s)H}. \tag{11}$$

Suppose that the output of the crystal reference can be described as

$$v(t)=\sqrt{2P}\sin\left(2\pi F_0 t+\varphi_0+\delta\varphi(t)\right), \tag{12}$$

where F_0 is the reference frequency, φ_0 is the initial phase, and $\delta\varphi(t)$ represents the oscillator phase noise. Assume S_φ represents the power spectrum of the oscillator phase noise. Recall that the output power spectrum of a linear system is expressed as

$$S_y(f) = S_x(f)\,|H(f)|^2, \tag{13}$$

where $S_x(f)$ is the input power spectrum and $H(f)$ is the linear system's transfer function (Stephens, 2002). Therefore, the output of the frequency synthesizer can be computed as

$$S_\phi(f) = S_\varphi(f)\left|\frac{1}{R}\frac{G(s)}{1+G(s)H}\right|^2. \tag{14}$$

The spectrum characteristic of the PLL is just like a narrow bandpass filter, of which the center is the output frequency of the PLL. Note that the bandwidth of the USO phase noise is far less than the loop bandwidth of the frequency synthesizer. As a result, according to the property of the PLL transfer function (which relates the VCO output to the crystal reference output), the action of the frequency synthesizer is just like a constant factor in the frequency domain. Consequently, we can conclude that

$$S_\phi(f) \approx S_\varphi(f)\frac{N^2}{R^2}. \tag{15}$$

Accordingly, in the time domain, the output phase noise of the frequency synthesizer caused by the oscillator phase noise can be approximately described as $N\cdot\delta\varphi(t)/R$.

Based on the characteristics of the PLL, by adjusting the parameters of the loop filter, the steady state error of the frequency synthesizer can achieve zero. As a result, the overall output instantaneous phase of the frequency synthesizer can be developed as

$$\theta_{\text{out}}(t) = \left(2\pi F_0 t + \varphi_0 + \delta\varphi(t)\right)\frac{N}{R}. \tag{16}$$

Therefore, Eq. (16) indicates that the single frequency synthesizer can be approximately treated as a phase multiplier.

3.1.2 Nested phase-locked loop

The structure of the nested PLL is shown in Fig. 3. It is formed by two signal PLLs. This novel construction is used to extract the reference frequency from the received carrier signal.

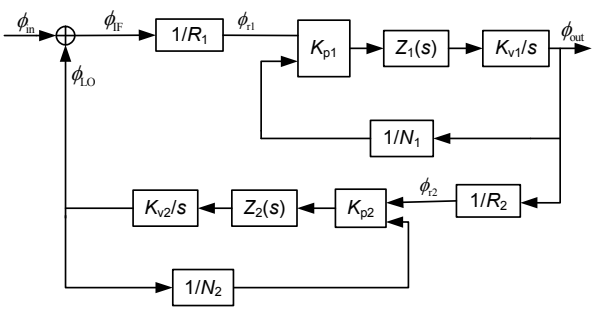

Fig. 3 Nested phase-locked loop (PLL) structure

Assume the input frequency to the nested PLL is f_{in}, and the output frequency of the nested PLL is f_{out}. When the nested loop is locked, the relationship between f_{out} and f_{in} can be derived as

$$\frac{f_{\text{out}}}{f_{\text{in}}} = \frac{1}{R_1/N_1 + N_2/R_2}. \tag{17}$$

Based on the control theory, the close loop transfer function can be expressed as

$$\frac{\Phi_{\text{out}}(s)}{\Phi_{\text{in}}(s)} = \frac{1}{\dfrac{R_1}{\text{CL}_1(s)} + \dfrac{\text{CL}_2(s)}{R_2}}, \tag{18}$$

where $\text{CL}_1(s)$ and $\text{CL}_2(s)$ each represents the single closed-loop transfer function (Wang *et al*., 2006).

Fortunately, the frequency characteristic of the nested loop is similar to that of the single loop. The oscillator phase noise lies mainly in the bandpass of the nested loop (Wang *et al*., 2006). According to the above analysis of the single PLL, the fluctuations (caused by oscillator instabilities) presented on the input and output of the nested loop are proportional to the instantaneous frequencies f_{in} and f_{out}. If the nested loop is properly designed, the steady state error will approach zero. As a result, the output instantaneous phase of the nested loop is proportional to the input instantaneous phase and the proportionality constant is numerically equivalent to $1/(R_1/N_1+N_2/R_2)$. In other words,

$$\frac{\phi_{\text{out}}}{\phi_{\text{in}}} = \frac{1}{R_1/N_1 + N_2/R_2},$$

where ϕ_{in} represents the input instantaneous phase and ϕ_{out} represents the output instantaneous phase of the nested loop.

3.2 Master satellite frequency planning

To avoid the same frequency interference, a thorough frequency planning is needed in designing the ranging system. In our design, to avoid the same frequency interference, the reference signal whose frequency is the same as the received signal is not generated directly. In fact, based on the property of the frequency synthesizer, we can simplify the reference signal-generating circuit branch by employing the intermediate frequency (IF) signal as the reference signal. The reason is disscussed in this section. Fig. 4 shows the front-end design of the master satellite, and the frequency parameters of different signals are shown in Table 1. The transmitted signal of the master satellite is produced in two stages: the IF stage and the radio frequency stage. Especially the IF signal has another role of serving as the reference signal. Note that the IF of the transmitter is just the same as the IF of the receiver.

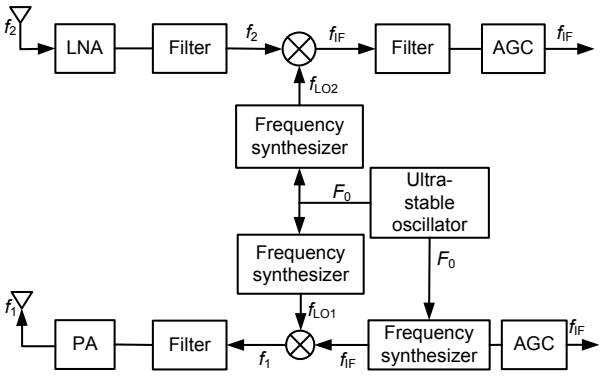

Fig. 4 Front-end of the master satellite
AGC: automatic gain control; LNA: low noise amplifier; PA: power amplifier

Table 1 Frequency parameters of different signals

Signal	Frequency parameter
Transmitted carrier	f_1
Received carrier	f_2
Local oscillator of the transmitter	f_{LO1}
Local oscillator of the receiver	f_{LO2}
Intermediate frequency signal	f_{IF}

Assuming the output signal of the USO is represented by Eq. (12), the instantaneous phase at a nominal time t can be expressed as $2\pi F_0 t+\varphi_0+\delta\varphi(t)$.

Fig. 4 shows that three frequency synthesizers are driven by the same USO. According to the property of the frequency synthesizer as Eq. (16) shows, the instantaneous phases of the three frequency synthesizers can be derived as

$$\begin{cases} \Psi_{LO1}=\left(2\pi F_0 t+\varphi_0+\delta\varphi(t)\right)\dfrac{f_{LO1}}{F_0}, \\ \Psi_{LO2}=\left(2\pi F_0 t+\varphi_0+\delta\varphi(t)\right)\dfrac{f_{LO2}}{F_0}, \\ \Psi_{IF}=\left(2\pi F_0 t+\varphi_0+\delta\varphi(t)\right)\dfrac{f_{IF}}{F_0}. \end{cases} \tag{19}$$

The radio frequencies f_1 and f_2 satisfy

$$\begin{cases} f_1=f_{LO1}+f_{IF}, \\ f_2=f_{LO2}+f_{IF}. \end{cases} \tag{20}$$

For any time t, the transmitted phase of the master satellite is represented as

$$\Psi_1=\left(2\pi F_0 t+\varphi_0+\delta\varphi(t)\right)\frac{f_1}{F_0}+C_1, \tag{21}$$

where C_1 represents the constant phase delay caused by the filter and mixer of the transmitter.

Assume the scaling transformation from the output phase to the input phase on the slave satellite can be completely achieved. Then, considering the flight time, the received phase of the master satellite is represented as

$$\Psi_2=\left(2\pi F_0(t-2\tau)+\varphi_0+\delta\varphi(t-2\tau)\right)\frac{f_2}{F_0}+C_2, \tag{22}$$

where C_2 represents the constant phase delay caused by the filter and other components, and f_2 represents the frequency of the received signal of the master satellite. Eq. (22) indicates that Ψ_2 contains the distance information.

Theoretically, the local reference instantaneous phase should have the following form:

$$\Psi_{ref}=\left(2\pi F_0 t+\varphi_0+\delta\varphi(t)\right)\frac{f_2}{F_0}. \tag{23}$$

Dual transponder phase measurement is defined as the subtraction of the two phases of Eqs. (22) and (23):

$$\Delta\Theta_{\mathrm{RF}}(t)=2\pi f_2\cdot 2\tau+\frac{f_2}{F_0}\big(\delta\varphi(t)-\delta\varphi(t-2\tau)\big)-C_2. \tag{24}$$

After the combination, most of the phase errors are canceled out except the short period variation having duration less than the TOF of the microwave signal. However, Eq. (24) has only a theoretical meaning because the measuring phase on a high frequency is difficult and it is not realizable in practice. As a result, the high frequency signal is usually converted to a low frequency signal for better processing.

Fig. 4 shows that the received signal is mixed with the local oscillator signal generated by the frequency synthesizer and the IF signal of the receiver is derived after filtering the output of the mixer. The instantaneous phase of the IF signal can be obtained by

$$\Theta_{\mathrm{IF}}=\Psi_2-\Psi_{\mathrm{LO2}}. \tag{25}$$

By substituting Eqs. (19), (20), and (22) into Eq. (25), the instantaneous phase can be represented by

$$\begin{aligned}\Theta_{\mathrm{IF}}=&2\pi f_{\mathrm{IF}}t-2\pi f_2\cdot 2\tau+\frac{f_{\mathrm{IF}}}{F_0}\varphi_0+\delta\varphi(t-2\tau)\frac{f_2}{F_0}\\&-\delta\varphi(t)\frac{f_{\mathrm{LO2}}}{F_0}+C_3.\end{aligned} \tag{26}$$

The phase difference between the IF signal of the transmitter and receiver can be expressed as

$$\Delta\Theta_{\mathrm{IF}}(t)=2\pi f_2\cdot 2\tau+\frac{f_2}{F_0}\big(\delta\varphi(t)-\delta\varphi(t-2\tau)\big)-C_3. \tag{27}$$

The difference between Eqs. (24) and (27) is just a constant. Therefore, based on the above analysis, we can simplify our design by just employing the IF signal of the transmitter as the reference signal as long as the IF signal (generated from a frequency synthesizer) of the transmitter and the local oscillator signal of the receiver are driven by the same USO.

3.3 Slave satellite frequency planning

The slave satellite just performs the scaling transformation from the received signal phase to the transmitted signal phase, and the transformation is continuous at all times. Fig. 5 shows the system-level structure of the slave satellite. f_1 and f_2 represent the frequency of the received signal and the transmitted signal, respectively.

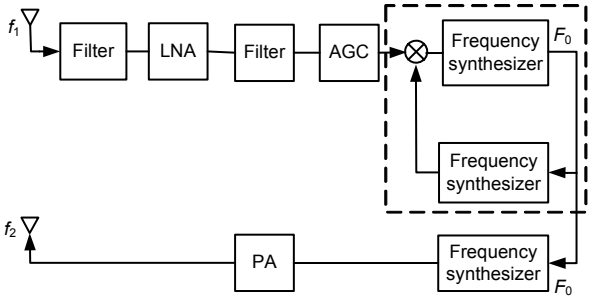

Fig. 5 Front-end of the slave satellite
AGC: automatic gain control; LNA: low noise amplifier; PA: power amplifier

From Fig. 5, we can see that the primary component is the frequency synthesizer; especially, the nested loop is constructed by two frequency synthesizers as indicated by the dashed line, and the detailed structure of the nested loop is shown in Fig. 3. The nested loop is used to recover the reference frequency from the received signal, and the recovered reference signal is used to drive the frequency synthesizer of the transmitter. The role of the recovered reference signal is just identical to the reference USO.

Based on the result of Eq. (17), the relationship $F_0=f_1/(R_1/N_1+N_2/R_2)$ can be easily satisfied as long as the frequency dividing ratios N_1, N_2, R_1, R_2 of the nested loop are properly selected. Likewise, the design of the transmitter frequency synthesizer also contains the selection of the frequency dividing ratios N_3, R_3 to meet the relationship $f_2=F_0\cdot N_3/R_3$. In a word, thorough frequency planning should go first and the frequency dividing ratios are selected accordingly.

The scaling transformation contains two stages: first of all, because of the nested loop, the reference signal is approximately derived from the received signal, and then through another frequency synthesizer driven by the recovered reference signal, the transmitted carrier centered at frequency f_2 is generated.

According to the above analysis, the instantaneous phase of the received signal can be expressed as

$$\Phi_1 = 2\pi f_1(t-\tau) + \left(\varphi_0 + \delta\varphi(t-\tau)\right)\frac{f_1}{F_0}, \qquad (28)$$

where τ is the flight time between the two satellites. Based on the characteristic of the nested loop analyzed above, the phase of the recovered reference signal can be approximated as

$$\Phi_{\text{ref}} = 2\pi F_0(t-\tau) + \varphi_0 + \delta\varphi(t-\tau). \qquad (29)$$

Based on the property of the frequency synthesizer, the transmitted phase of the slave satellite can be derived as

$$\Phi_2 = 2\pi f_2(t-\tau) + \left(\varphi_0 + \delta\varphi(t-\tau)\right)\frac{f_2}{F_0}. \qquad (30)$$

The scaling factor $k=\Phi_2/\Phi_1$ is a constant whose value is f_2/f_1. Therefore, k can be derived as

$$k = \frac{N_3 / R_3}{R_1 / N_1 + N_2 / R_2}. \qquad (31)$$

Note that k is determined only by those division factors of the slave satellite, and its value has nothing to do with f_1 and f_2. Since f_2 satisfies the relationship $f_2=kf_1$, f_2 is proportional to f_1 accordingly.

In summary, it is easily observed that the slave satellite does not have its own USO, and the reference signal it needs is recovered from the received carrier. In this sense, the whole ranging system is driven by only one USO. In fact, the slave satellite just completes coherent transfer while keeping synchronization. From the system-level analysis above, we conclude that the scaling transformation can be accomplished with negligible degradation in fractional frequency stability.

3.4 Dynamics consideration

The above analysis is based on the premise that the two satellites keep a constant distance moving towards the same direction. Nevertheless, there is relative motion between the two satellites as they travel in space. Therefore the characteristic of dynamics must be taken into consideration at the preliminary design stage of the ranging system.

When considering the dynamics, the primary modification in our design is the frequency synthesizer parameters, especially the order of loop filter which directly determines the dynamic property. The bandwidth and the order of the closed-loop transfer function must be adjusted according to the tracking property caused by dynamic range changes between the twin satellites. Conventionally, the third order PLL provides the desirable characteristic of being able to track an accelerating frequency input (Stephens, 2002).

Assume the instantaneous Doppler frequency has the form (Aguirre and Hurd, 1984)

$$f_{\text{d}}(t) = \frac{f_{\text{c}}}{c}(\Omega_0 + \Lambda_0 t), \qquad (32)$$

where f_{c} is the carrier frequency (Hz), c is the speed of light (m/s), Ω_0 is the relative velocity between two satellites (m/s), and Λ_0 is the relative acceleration between two satellites (m/s^2).

The steady-state phase error for this loop caused by Doppler effects can be calculated via the final-value theorem, and is

$$\phi_{\text{ss}} = \lim_{s\to 0}\frac{2\pi f_{\text{c}}}{c}\left(1-H(s)\right)\left(\frac{\Omega_0}{s^2} + \frac{\Lambda_0}{s^3}\right), \qquad (33)$$

where $H(s)$ is the closed-loop transfer function of control loops. To control the steady-state phase error to a minor acceptable level and to meet the tracking property caused by dynamics, parameters of the frequency synthesizer in our design must be properly selected. Traditionally, the parameters are set according to the worst condition, and $\phi_{\text{ss}}=0$ is recommended to guarantee the complete scaling transformation.

As for the frequency planning of the master and slave satellites, the Doppler frequency must be taken into account. Based on the above analysis, how the ranging system responds to Doppler effects is disscussed.

The incoming frequency to the slave satellite varies by Doppler effects. Assuming the relative velocity is R, the incoming frequency can be expressed as

$$f_1' = f_1\left(1+\frac{R}{c}\right), \qquad (34)$$

where f_1 is the transmitted frequency of the master satellite.

According to Eq. (31), the scaling factor k remains unchanged as long as the division factors of the frequency synthesizers in Fig. 5 are kept fixed at a predetermined value. Assuming complete scaling transformation, the transferred frequency of the slave satellite can be expressed as

$$f_2' = kf_1\left(1+\frac{R}{c}\right). \tag{35}$$

Considering the Doppler effects, the received frequency of the master satellite can be expressed as

$$f_2 = f_2'\left(1+\frac{R}{c}\right) = kf_1\left(1+\frac{R}{c}\right)^2 = kf_1\left(1+\frac{2R}{c}+\frac{R^2}{c^2}\right). \tag{36}$$

Since $R \ll c$, f_2 can be approximated by

$$f_2 = kf_1\left(1+\frac{2R}{c}\right). \tag{37}$$

So, the Doppler frequency extracted on the master satellite is

$$f_\mathrm{d} = kf_1\left(\frac{2R}{c}\right). \tag{38}$$

The useful dynamic information is contained in f_d. Since the received signal f_2 contains the Doppler frequency, the IF contains the Doppler frequency accordingly. However, since the Doppler frequency can be extracted using digital PLL, the electrical structure of the master satellite remains unchanged. The only change is that the IF of the upper branch in Fig. 4 should change from f_IF to $f_\mathrm{IF}+f_\mathrm{d}$.

In conclusion, when considering the dynamics, the above analysis of the frequency planning needs some modifications. Primarily, in this case, the frequency of the reference signal recovered from the received signal contains a fractional Doppler frequency. However, the system-level structure remains the same as in the motionless condition.

The dynamics are not discussed in detail here since the objective of this paper is to illustrate the design of a dual transponder ranging system.

4 System demonstration

To verify the feasibility of the dual transponder ranging system and the effectiveness of oscillator noise cancellation, a ranging system demonstration is needed. Based on the design analysis discussed above, the ranging platform is built. In reality, the actual inter-satellite distance varies from several kilometers to several hundred kilometers in space. On the one hand, the multipath effect is rare in space while inevitable on the ground (because of the complex environment) and can severely affect the ranging accuracy if simulating a long distance on the ground. On the other hand, short inter-satellite distance does not affect the feasibility validation of the designed system. Compared with the short distance between satellites, the long distance only means longer flight time of the signal and more attenuation of the signal power. With respect to power attenuation, signal power can be easily controlled with the aid of power attenuators. As to the flight time, according to Eq. (6), it merely affects the cancellation effect of oscillator noise. Therefore, the main difference between the short and long separations is related to the level of oscillator noise suppression. The shorter the separation distance, the more the cancellation of oscillator noise, resulting in a little higher ranging accuracy. Since we aim to verify the feasibility of the designed dual transponder ranging system, the priority is focused on the assumption validation of oscillator noise suppression. To keep the multipath effect to a minor level, we choose a separation distance of about 5 m temporarily for all tests and the power attenuation is set to a large scale according to the long separation. Some parameters are set in Table 2.

Table 2 Platform parameter configuration

Parameter	Value
Phase frequency band, S (GHz)	2.4
Effective wavelength (cm)	6.25
Allan variance of the ultra-stable oscillator	1×10^{-11}/(100 s)
Scaling factor k	240/200
Inter-satellite distance (m)	5

The assembled demonstration system containing the master and the slave satellite modules is made up of readily available components. The block diagram is similar to the demonstration by Macarthur and Posner (1985). The antennas of the two satellites are fixed on each side of the moveable platform with one system fixed and the other moveable as shown in Fig. 6. The antenna is connected to both the transmitter and receiver of the satellite through a triple ports circulator. In other words, the two antennas work in duplex mode. Accordingly, the transponder works under wireless condition in this experiment. To alleviate multipath effects, we chose antennas with good directivity and an open area. The motion of the moveable platform can be controlled precisely by means of a programming controller. Its motion is linear in one direction and the precision can reach the μm-level. By adjusting the position of the movable platform with the μm-level step, the phase between the master and slave satellites is set to simulate a particular range separation, or time delay.

According to Fig. 4, the measurement phase is obtained on the master satellite. After the preprocessing of the front-end of the master satellite, the two IF signals are sampled and the samples are delivered to the field programmable gate array (FPGA) and digital signal processing (DSP) for post-processing to extract the measurement phase (Thomas, 1989; Yang *et al*., 2010). Next, a sophisticated filter algorithm is designed to remove the undesired noise, and at last, the phase data are converted to an equivalent range using the known effective wavelength. The filter used in dual transponder ranging is the least-square filter. It is a well-known technique of fitting a quadratic function by least squares to the range values to extract range. For more information, one may refer to Thomas (1999). Finally, a computer-based data collection system makes our further analysis of the measurement range available and the obtained test results are provided graphically.

Since there is no information of integer ambiguity in the experiment, all the ranging results lie in an effective wavelength. Fig. 7 shows the dual transponder ranging result of the twin satellites under the motionless situation. We can see that the error level is very low when all of the error sources (such as oscillator noise, multipath noise, and system noise) are applied, root mean square (rms) of 32 μm.

In contrast to dual transponder ranging, the single one-way ranging result is also provided in Fig. 8. The measuring conditions are set nearly the same as the dual transponder ranging measurement except that

Fig. 6 Motion apparatus for the demonstration system

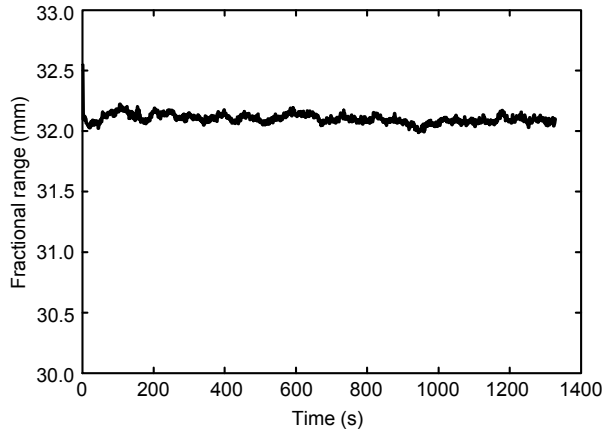

Fig. 7 Dual transponder ranging result under motionless situation

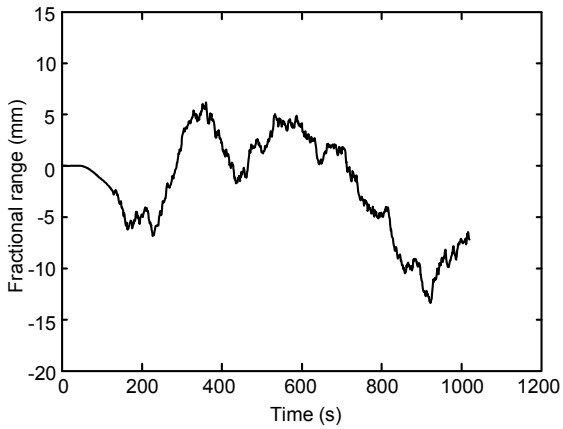

Fig. 8 Single one-way ranging result under motionless situation

it does not need the reference signal. The error level is becoming worse, rms of 4.8 mm. By comparison with the single one-way ranging measurement, significant improvements of the error level in the dual transponder carrier ranging are obtained. Besides, from Figs. 7 and 8, we can infer that other error sources have little effect compared with the oscillator noise.

Fig. 9 shows the dual transponder ranging result under a uniform motion situation. The velocity of the movable platform is set at 40 μm/s. Dependent range measurements are obtained when the platform moves smoothly toward one direction. The slope of the plotted time-series in Fig. 9 represents the measurement velocity and the period characteristic just represents the cycle-skipping. By subtracting successive measurements, the derived measurement velocity is almost equal to the value set in advance and the range-rate error level can be estimated, rms of 7.5 μm/s .

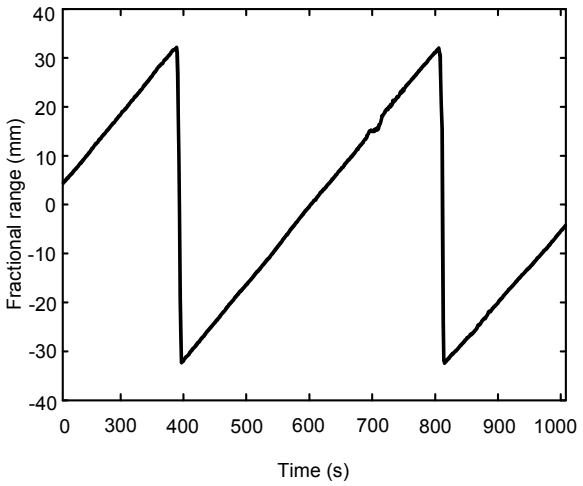

Fig. 9 Dual transponder ranging result under uniform motion situation

Consequently, we can conclude that the dominant error source in the inter-satellite ranging system is caused by oscillator instability and the dual transponder ranging system is effective in cancellation of the oscillator noise. Furthermore, the feasibility of the novelty design scheme of the dual transponder ranging system is also verified.

5 Conclusions

The dual transponder carrier ranging system is described and it determines the distance within an effective wavelength (Eq. (8)) with a high precision. To handle integer ambiguity, we draw support from other means (such as pseudo-noise ranging). The derived ranging measurement equation shows that the dual transponder ranging system can remove most of the oscillator noise effectively and the accuracy of the dual transponder ranging system can reach as high as that of the dual one-way ranging system theoretically. Based on the principle of the dual transponder ranging system along with the property of the frequency synthesizer, a detailed design method of the ranging system is put forward and the supporting analysis illustrates the feasibility of this approach. A laboratory demonstration system is assembled to verify the performance of the dual transponder ranging system. The experimental results demonstrate that a high level of ranging accuracy can be achieved (about 30 μm under the laboratory circumstance) by the use of the dual transponder ranging system. Besides, unlike the dual one-way ranging system, the dual transponder ranging system does not need to rely on the time tagging system to synchronize the two satellites since the measurement phase is derived on only one satellite. As a result, dual transponder ranging may be used for other planets which do not have GPS in future missions. Furthermore, it may benefit formation flying missions that require real-time high accuracy inter-satellite ranging measurements.

References

Aguirre, S., Hurd, W.J., 1984. Design and Performance of Sampled Date Loops for Subcarrier and Carrier Tracking. The Telecommunications and Data Acquisition Progress Report 42-79, Jet Propulsion Laboratory, Pasadena, Calif.

Bertiger, W., Bar-Sever, Y., Desai, S., Dunn, C., 2002. GRACE: Millimeters and Microns in Orbit. Proc. ION GPS, Institute of Navigation, p.2022-2029.

Bertiger, W., Dunn, C., Harris, I., Kruizinga, G., Romans, L., Watkins, M., Wu, S., 2003. Relative Time and Frequency Alignment Between Two Low Earth Orbiters, GRACE. Proc. IEEE Int. Frequency Control Symp. and PDA Exhibition Jointly with the 17th European Frequency and Time Forum, p.273-279. [doi:10.1109/FREQ.2003.1275101]

Dean, B., 2003. PLL Performance, Simulation and Design. National Semiconductor, p.88-150.

Kim, J., 2000. Simulation Study of a Low-Low Satellite-to-Satellite Tracking Mission. PhD Thesis, University of Texas at Austin, USA.

Kim, J., 2007. Measurement Time Synchronization for a Satellite-to-Satellite Ranging System. Proc. Int. Conf. Control, Automation and Systems, p.190-194.

Kim, J., Tapley, B.D., 2002. Error analysis of a low-low satellite-to-satellite tracking mission. *J. Guid. Control Dyn.*, **25**(6):1100-1106. [doi:10.2514/2.4989]

Kim, J., Tapley, B.D., 2003. Simulation of dual one-way ranging measurements. *J. Spacecraft Rockets*, **40**(3): 419-425. [doi:10.2514/2.3962]

Kim, J., Tapley, B.D., 2005. Optimal frequency configuration for dual one-way ranging systems. *J. Spacecraft Rockets*, **42**(4):749-751. [doi:10.2514/1.9974]

Macarthur, J.L., Posner, A.S., 1985. Satellite-to-satellite range-rate measurement. *IEEE Trans. Geosci. Remote Sens.*, **23**(4): 517-523. [doi:10.1109/TGRS.1985.289443]

Stephens, D., 2002. Phase-Locked Loops for Wireless Communications (2nd Ed.). Kluwer Academic Publishers, p.47-56, 353-400.

Thomas, J.B., 1989. An Analysis of Digital Phase-Locked Loops. JPL Publication 89-2, Pasadena, CA.

Thomas, J.B., 1999. An Analysis of Gravity-Field Estimation Based on Inter-Satellite Dual-1-Way Biased Ranging. JPL Publication 98-15, Pasadena, CA.

Wang, C.H., Yu, F.X., Jin, Z.H., Zheng, Y.M., Zhao, X.Y., 2006. Research on noise of TT&C transponder for pico-satellites. *Syst. Eng. Electr.*, **28**(12):1514-1517 (in Chinese).

Yang, J., Yang, Y.K., Liang, L.F., Liu, L., 2010. Research on Digital Phase-Locked Loop about K/Ka-Band High Precision Receiver. Proc. Int. Intelligent System Design and Engineering Application Conf., p.185-188. [doi:10.1109/ISDEA.2010.171]

Zhao, X.Y., Jin, X.J., Jin, Z.H., 2009. Simulation of dual transponder carrier ranging measurements. *J. Zhejiang Univ.-Sci A*, **10**(10):1395-1403. [doi:10.1631/jzus.A0820802]